6-5-2018

# Controllable Internal Mixing in Coalescing Droplets Induced by The Solutal Marangoni Convection of Surfactants with Distinct Headgroup Architectures

Jerome J. Nash

Patrick T. Spicer

Kendra Erk

# Controllable internal mixing in coalescing droplets induced by the solutal Marangoni convection of surfactants with distinct headgroup architectures

Jerome J. Nash[a], Patrick T. Spicer[b], and Kendra A. Erk[a*]

a. School of Materials Engineering, Purdue University, West Lafayette, IN 47907, USA;

b. School of Chemical Engineering, The University of New South Wales, Sydney 2052, Australia

[*]corresponding author, Email: erk@purdue.edu, Phone: (765) 494-4118

**Keywords:** Marangoni flow; convection; mixing; coalescence

## Abstract

Through several complementary experiments, an investigation of the bulk and interfacial flows that emerged during the coalescence of two water-in-oil droplets with asymmetric compositional properties was performed. By adding surfactant to one of the coalescing droplets and leaving the other surfactant-free, a strong interfacial tension gradient (i.e., solutal Marangoni) driving energy between the merging droplets generated pronounced internal mixing. The contributions of two distinct types of surfactant, anionic ammonium lauryl sulfate (ALS) and cationic cetyltrimethylammonium bromide (CTAB) on the rate of coalescence bridge expansion and on the generation of opposing flows during coalescence were investigated. All coalescence experiments supported the power law relation between the radius of the expanding connective liquid bridge and time, $r_b \propto t^{1/2}$. However, the presence of surfactant decreased the magnitude of the prefactor in this relationship due to induced interfacial solutal Marangoni convection. Experiments showed that packing efficiency, diffusivity, and bulk concentration of the selected surfactant are vital in solutal Marangoni convection and thus the degree and timescale of internal mixing between merging droplets, which has yet to be adequately discussed within the literature. Denser interfacial packing efficiency and lower diffusivity of CTAB produced stronger opposing

bulk and interfacial flow as well as greater bulk mixing. A discussion of how optimized surfactant selection and solutal Marangoni convection can be used for passively inducing convective mixing between coalescing drops in microfluidic channels when viscosity modulation is not feasible is provided.

## Graphical Abstract

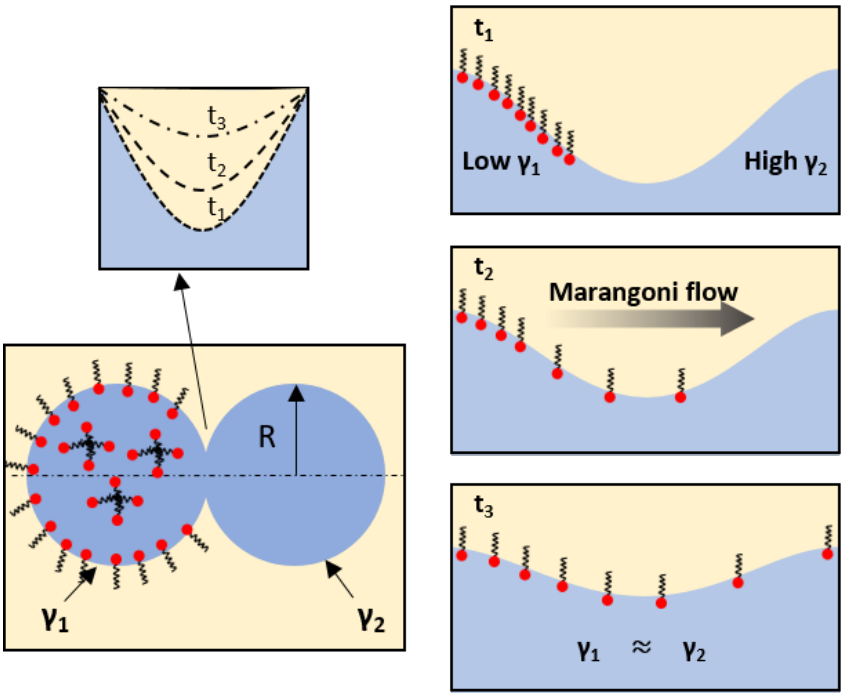


## 1. Introduction

The coalescence of two identical droplets, and the corresponding bulk fluid flows that emerge, has been studied at length in the literature. [1–5] However, far less attention has been given to the coalescence of binary droplets with asymmetric physical properties, despite its importance to many industrial and research applications including enhanced oil recovery [6], emulsification [7], microfluidic reactors [8], and functional microparticle fabrication. [9–11]

Many additional examples can be found in the literature of microfluidic applications that utilize the coalescence of droplets as a vital processing step in material fabrication. However, mixing immiscible phases in microfluidic devices often proves difficult because of the low

Reynolds number flows encountered within microchannels. Several researchers have shown that the combination of immiscible fluids in microchannels can be improved with modified channel designs [12–14] or, quite often, by modulating the viscosity of one or both of the coalescing fluids to achieve desired bulk convective mixing. [15,16] While several detailed coalescence studies have investigated the effects of variable external oil phase viscosity on the generation of bulk flows in coalescing water droplets [17,18], little attention was given to the potential influence of polar surfactant headgroup architecture in the generation of the observed opposing interfacial and bulk flows. Moreover, altering the viscosities of the bulk fluids is not always a viable option in microfluidic applications (for example, when high throughput is a processing requirement, or when a system is restricted to fluids with predetermined viscosities). Thus, additional routes for inducing a similar degree of internal mixing under these restrictions are necessary, and currently, no experimental studies in the literature have sought to provide insight into how appropriate surfactant selection can influence this phenomenon.

Utilizing solutal Marangoni convection, also known as the Gibbs-Marangoni effect, [19,20] provides a compelling avenue for inducing desired bulk flows in coalescing binary fluid systems, without the need for modulating bulk fluid viscosity. The Gibbs-Marangoni effect can be induced simply by adding a dilute concentration of a highly surface-active solute to one of the fluid droplets, while keeping the second drop initially free of any surfactant, then bringing the droplets into contact. When the two fluid droplets coalesce, a highly curved connective liquid bridge forms between them and expands rapidly due to interfacial stresses. In the inertial regime, a scaling relation derived from a simple physical argument can be used to describe the expansion of the coalescence bridge. [4] This scaling law predicts linear proportionality between the radius of the connective liquid bridge, $r_b$ (= $D_b/2$), and the square root of the coalescence time, $t^{1/2}$, given

by the equation, $D_b/2 \propto (R\gamma/\rho_{out})^{1/4}t^{1/2}$, where R is the initial drop radius, $\gamma$ is the interfacial tension, and $\rho_{out}$ is the density of the outer fluid.

As bridge expansion proceeds, the resulting fluid motion acts to pull the droplets together to form a single, larger drop. However, in the presence of an induced surface tension (i.e., surfactant concentration) gradient between the droplets, opposing interfacial and bulk flows can emerge. This is because surfactant molecules become nonuniformly distributed at the interface along the highly curved, connective liquid bridge separating the surfactant-laden and surfactant-free drops. [21] Relaxation to a homogenous surfactant coverage does not proceed primarily by diffusion, but by a far more rapid process (i.e., the Gibbs-Marangoni effect) where the surfactant molecules at the interface swiftly migrate toward regions of highest local interfacial tension. This in turn generates interfacial motion in the direction of the surfactant concentration gradient that acts tangentially to the merging droplets, which is accompanied by bulk motion in the adjacent fluid layers. Consequently, bulk flows which drive the droplets together under the influence of a favorable reduction in capillary pressure, $\Delta P = 2\gamma/R$, become unbalanced with interfacial flows. This ultimately results in opposing interfacial and bulk convective motion and can lead to pronounced bulk fluid mixing.

It has been shown that the mobility [22], as well as the degree of equilibrium interfacial adsorption of low molecular weight surfactants [23,24], can vary substantially depending on the nature of the surfactant's polar headgroup in a polar solvent such as water (i.e., whether it is anionic, cationic, nonionic, or zwitterionic). These interfacial characteristics are also well-known to have demonstrated importance in the occurrence of film rupture and coalescence for surfactant-laden fluid interfaces. [25,26] Therefore, it would stand to reason that strategically modulating the interfacial mobility, equilibrium saturation adsorption, and adsorption-desorption kinetics of the

added surfactant would enable interested parties to control coalescence related phenomena, such as passively-induced internal mixing between emulsion droplets in the presence of a surfactant concentration gradient. Optimized design of such small-scale processes will require the ability to identify appropriate surfactants based on their physicochemical properties and performance in applications like diagnostic chips and other microfluidics systems. Thus, this work seeks to demonstrate several key mechanisms relating the adsorption of two oppositely charged ionic surfactants and the manifested solutal Marangoni flows that drive bulk mixing between coalescing aqueous droplets in a viscous surrounding oil. Generalized relationships between the interfacial properties of low molecular weight surfactant and their potential influence on bulk coalescing phenomena are also provided.

Many detailed experimental and theoretical analyses have been performed which elucidate early-stage coalescence phenomena of uniform liquid droplets both in air and an external liquid. [1–5] However, fully developed mixing behaviors in the later stages of coalescence (i.e., several milliseconds following the onset of coalescence) are often a primary concern in microfluidic reactor applications. [8,27] Therefore, to aid in the design of such systems, the specific aims of this work were to (1) investigate the late-stage coalescence behavior of binary liquid droplets with an induced surfactant concentration gradient along the connective liquid bridge, and (2) illustrate how controlling equilibrium adsorption and solutal Marangoni motion through appropriate surfactant selection can encourage varying degrees of bulk fluid mixing. Through several complementary experiments, including equilibrium surfactant adsorption measurements, high-speed image processing, and concentration gradient-induced interfacial velocity measurements via particle tracking, we provide new insights into the fundamental relationships between optimized surfactant selection and bulk fluid mixing. Considering that the adsorption and interfacial

spreading behavior of surfactants can vary dramatically depending on the electrostatic interactions of the surfactant present at the fluid interface in the bulk aqueous solution [28], detailed investigations which further elucidate the role of surfactant selection in the development of varying degrees of opposing flows within coalescing binary droplets are essential.

## 2. Materials and Experimental Methods

### *2.1. Materials*

The external liquid phase used during drop coalescence measurements was a triglyceride oil (Stepan Company, CAS # 73398-61-5) with a manufacturer reported viscosity of 25 mPa·s and density of 0.95 g $cm^{-3}$, both at 25 °C. The oil was double-filtered through a chromatography column containing alumina (Fisher, CAS # 1344-28-1) to remove trace surface-active impurities prior to use. The droplets consisted of aqueous solutions prepared with water passed through a Filmtec™ reverse osmosis membrane (total dissolved solids ≤ 15 ppm, Dow Chemical Company). The two commercially available surfactants used in this study, ammonium lauryl sulfate, ALS (anionic surfactant, 30% in water, CAS # 2235-54-3) and cetyltrimethylammonium bromide, CTAB (cationic surfactant, ≥ 99%, CAS # 57-09-0), were obtained from Sigma-Aldrich and used without further purification. The blue dye added to the surfactant-free droplet in each binary droplet coalescence measurement as an aid for visualizing bulk motion was purchased from Queen Fine Foods Pty Ltd. The flat metal capillaries (18-gauge x 1.0" blunt tip dispensing needles) used in droplet coalescence experiments were obtained from CML Supply.

### *2.2. Visualizing rapid binary drop coalescence*

A schematic of the experimental setup used for visualizing binary liquid droplet coalescence is shown in Figure 1. Experiments were performed using a pair of three-axis

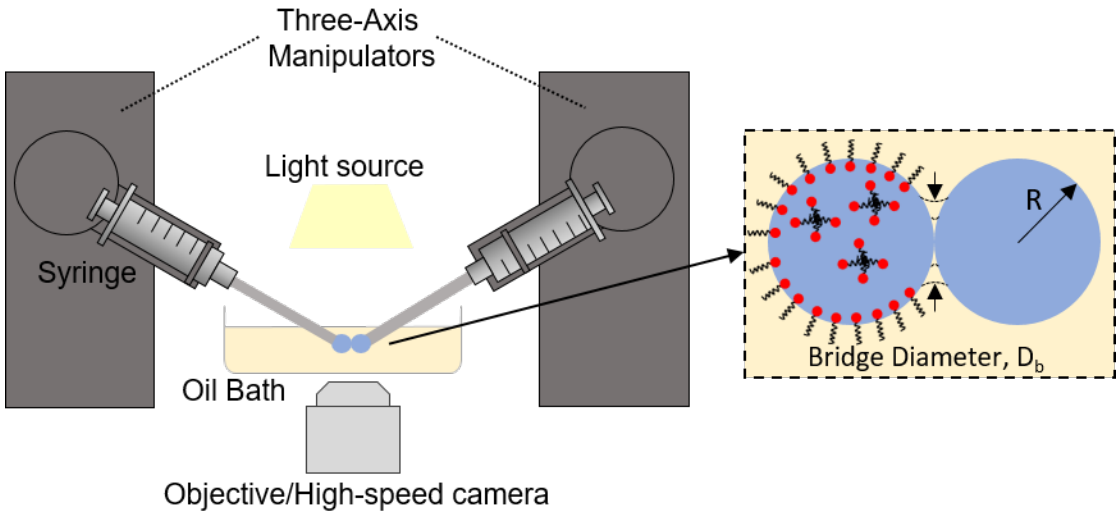


**Figure 1.** An illustration of the experimental setup used to study coalescence phenomena between binary aqueous droplets in a surrounding oil. The leftmost aqueous droplet was laden with surfactant and the rightmost droplet was surfactant-free, yet contained a small concentration of dye to aid in flow visualization.

micromanipulators (Sensapex) secured to z-axis translational stages (THORLABS) flanking an inverted optical microscope (AE31, Motic Microscopes). Two water droplets with asymmetric compositional properties, each having an initial diameter of 2 mm (unless otherwise specified) were formed at the tips of 18-gauge metal capillaries and were made to contact at negligible approach velocities (~0.01 mm $s^{-1}$) in a clear petri dish containing the low viscosity triglyceride oil (5 mL working volume). Coalescence of the binary droplets was captured with a high-speed camera (Phantom v7.3) at 11000 frames per second. Measurements of the bridge expansion kinetics were performed via image processing using open-source ImageJ software. [29]

A concentration gradient along the connective liquid between the two merging water drops was generated by adding the surfactant of interest to the leftmost coalescing droplet (Figure 1), while keeping the rightmost droplet surfactant-free. The surfactant-loaded droplet in each experiment contained either ALS or CTAB at a concentration of $2.5\times10^{-3}$ mol $L^{-1}$, which was near the experimentally determined critical micelle concentration (CMC) for each surfactant type. The relevant data used in determining the CMC for each surfactant is provided in Section 2.3. This

initial bulk surfactant concentration was chosen because near and above the CMC, the chemical potential of the surfactant negligibly changes and as a result conditions at the interface do not change. [30] Thus, the surfactant-laden droplet interface in this experimental setup represents an interfacial monolayer near saturation equilibrium. At the chosen bulk concentration, the equilibrium interfacial tension of the oil-water interface was $3.40 \pm 0.48$ mN $m^{-1}$ for ALS and $3.01 \pm 0.41$ mN $m^{-1}$ for CTAB, as determined by the drop shape analysis technique (Section 2.3).

To help visualize the emergent bulk fluid motion during droplet coalescence, dye was added to the surfactant-free droplet at a concentration of 0.1 g $L^{-1}$. The addition of dye did not substantially affect the oil-water interfacial tension (surfactant-free, pure droplet: $\gamma = 23.67 \pm 0.13$ mN $m^{-1}$; surfactant-free, dyed droplet: $\gamma = 21.42 \pm 0.27$ mN $m^{-1}$), and thus its contribution to the emergent coalescence flows was presumed to be negligible in comparison to the presence of the highly surface-active molecules, ALS and CTAB.

*2.3. Determination of interfacial adsorptive properties at the oil-water interface*

Interpreting the relationship between the induced bulk flows and the contributing interfacial Marangoni stresses of coalescing binary droplets requires knowledge of the equilibrated interfacial adsorption for each surfactant-laden droplet prior to merging. The effective interfacial tension values for pure and surfactant-laden oil-water interfaces were obtained using axisymmetric drop shape analysis with a contact angle goniometer/tensiometer (Ramé-Hart) following experimental procedures established in previous work by Nash and Erk. [31] The theory underpinning this technique and its corresponding application to study the effective interfacial tensions for air-liquid and liquid-liquid monolayers have been previously discussed in the literature. [32,33] In brief, the interfacial tension of each oil-water interface was determined by fitting the shape profile of an aqueous pendant drop suspended from the tip of a flat 12-gauge

PTFE capillary immersed in oil to the theoretical profile prescribed by the Young-Laplace equation, $\Delta P = \gamma\left(\frac{1}{R_1} + \frac{1}{R_2}\right)$. This force balance relates the differential in pressure, $\Delta P$, across a curved interface to its principle radii of curvature $R_1$ and $R_2$, and interfacial tension, $\gamma$. As surface active solutes become adsorbed to the interface, there is a demonstrable reduction in the capillary pressure. For a known pressure and interfacial curvature, the effective interfacial tension of the surfactant-laden interface can be directly measured.

The equilibrium interfacial adsorption isotherms for dilute aqueous solutions of ALS or CTAB in contact with triglyceride oil are provided in Figure 2. In each adsorption experiment, the interfacial tension was measured over time for at least 45 minutes, or until a constant interfacial tension value was reached. The critical micelle concentration (CMC's) for each surfactant was determined graphically from Figure 2 as the intersection of the linear fits to the low and high

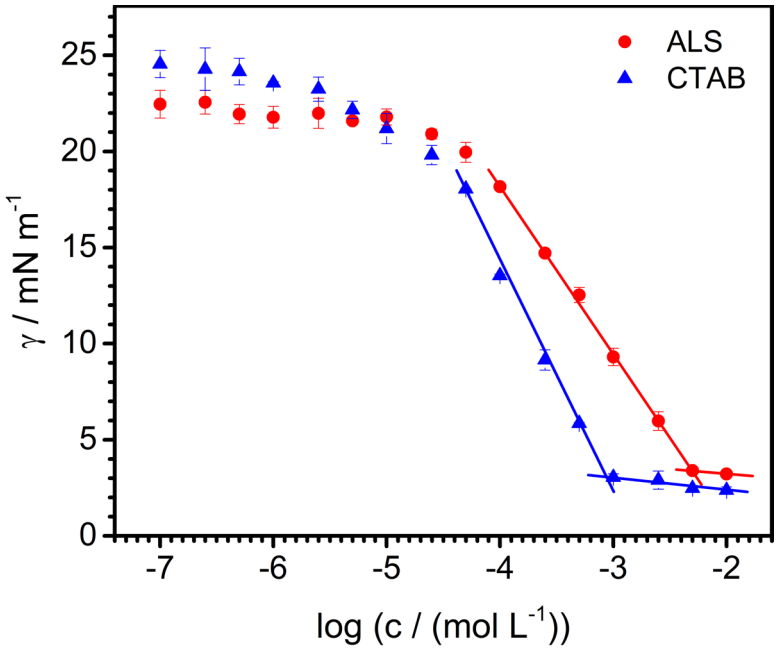


**Figure 2.** Interfacial tension, γ, versus log of surfactant concentration, c, in aqueous solution at 23 °C at the triglyceride oil-water interface measured by the drop shape analysis technique. Lines represent best-fitting straight fitting line in the low surfactant concentration regime was used in the determination of the surface excess

concentration regimes for each surfactant. Experimental CMC values for ALS and CTAB at 23 °C were ca. $5.5\times10^{-3}$ mol $L^{-1}$ and $0.95\times10^{-3}$ mol $L^{-1}$, respectively. The CMC value obtained here for ALS closely corresponded to the value found in the literature, $6.25\times10^{-3}$ mol $L^{-1}$. [34] Likewise, the CMC value obtained here for CTAB agreed well with previous observations in the literature of $0.9\times10^{-3}$ mol $L^{-1}$ [35] and $1\times10^{-3}$ mol $L^{-1}$ [36].

The surface excess concentration, $\Gamma_m$, corresponds to the maximum concentration of surfactant adsorbed to the oil-water interface of the surfactant-laden droplet at equilibrium and was approximated for each surfactant using the Gibbs adsorption equation, $\Gamma_m = -\frac{1}{mRT}\left(\frac{d\gamma}{d\log c}\right)_{T,P}$, where $\gamma$ is the interfacial tension (mN $m^{-1}$), c is the bulk surfactant concentration (mol $L^{-1}$), R is the gas constant, T is the temperature (K), and the integer, m, accounts for the charge interactions within the polar head group of the surfactant. For dilute aqueous solutions containing a single, 1:1 ionic surfactant in the absence of excess salt, m = 4.606, which was taken for both anionic ALS and cationic CTAB. [37,38] Substituting the slope value of the best-fitting straight line in the low surfactant concentration regime from the interfacial tension versus log of surfactant concentration curve for $\frac{d\gamma}{d\log c}$ in the Gibbs adsorption equation, $\Gamma_m$ was calculated for ALS and CTAB at the triglyceride oil-water interface. The minimum molecular area, $A_{min}$ ($Å^2$ $molecule^{-1}$), was then determined from the equation, $A_{min} = \frac{1\times10^{20}}{\Gamma_m N_A}$, where $N_A$ is Avogadro's number. (Table 1).

**Table 1.** Surface excess concentrations and minimum molecular areas calculated for ALS and CTAB at 23 °C at the triglyceride oil-water interface.

| Surfactant | Surface Excess Concentration, $\Gamma_m/(10^{-6}$ mol $m^{-2})$ | Minimum Molecular Area, $A_{min}/(Å^2$ $molecule^{-1})$ |
|---|---|---|
| Ammonium Lauryl Sulfate (ALS) | 0.76 | 218 |
| Cetyltrimethylammonium bromide (CTAB) | 1.07 | 156 |

194 *2.4. Determination of surfactant-induced interfacial spreading velocity, $U_s$*

195 The experimental setup used to study the interfacial spreading velocity, $U_s$, of each
196 surfactant when introduced into the pure triacylglyceride oil-water interface is shown in Figure 3.
197 The displacement of tracer particles (hollow glass spheres, 9-13 μm diameter, Sigma-Aldrich,
198 CAS # 65997-17-3) seeded at the pure oil-water interface initiated by the introduction of a
199 surfactant-loaded water droplet to the pure oil-water interface and driven by solutal Marangoni
200 flow was measured.

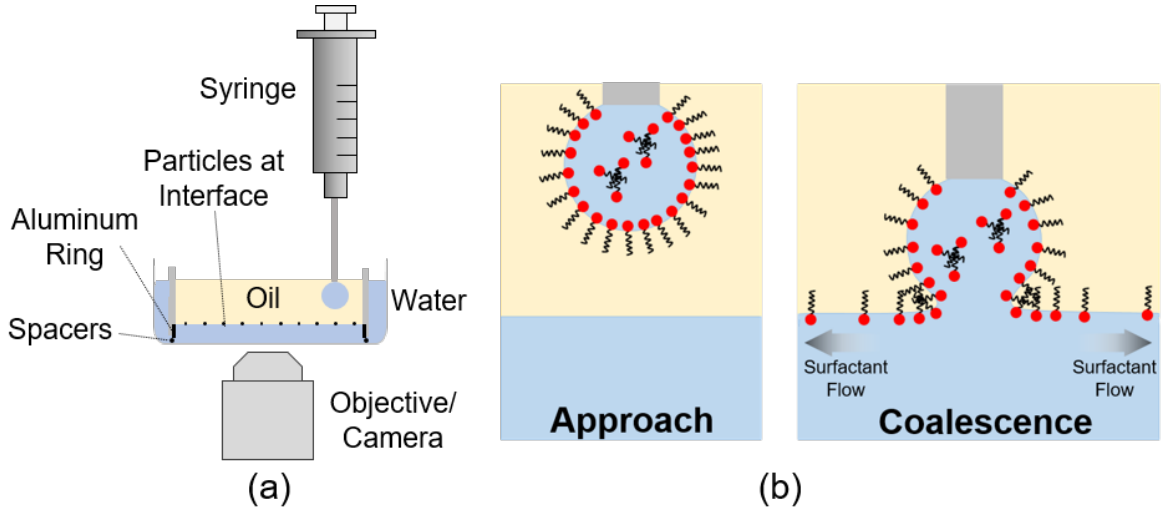


**Figure 3.** Schematic representation of the experimental setup used to quantify interfacial spreading velocities, $U_s$, under an induced interfacial tension gradient at the triglyceride oil-water interface. A side view depicting the introduction of a surfactant loaded water droplet at the surfactant-free, oil-water interface (containing tracer particles) is shown in (a) and an illustration of the surfactant diffusion mechanism, quantified by measuring the rate of displacement for tracer particles attached to the interface, is shown in (b).

201 The motion of tracer particles was measured at a planar oil-water interface because this
202 experimental scheme specifically enabled the measurement of Marangoni-induced flow rates
203 under the effect of a surfactant concentration gradient at the oil-water interface. Ensuring that the
204 measured flow rates were obtained for tracer particles located specifically at the oil-water interface
205 and not within one of the subphases was most directly accomplished with a droplet coalescing with
206 a planar oil-water interface.

Preparation of a planar triglyceride oil-water interface containing the seeded glass spheres was performed using a modified optical microscopy cell and methodology adapted from the work of Park et al. [39] The cell used here consisted of a polystyrene petri dish (height 1 cm, outer diameter of 40 mm) and a concentric polystyrene cylinder (height 1 cm, outer diameters of 30 mm). An aluminum ring was inserted into the bottom of the inner polystyrene cylinder to pin the contact line of the oil-water interface. The inner cylinder was secured to the polystyrene petri dish using a fast curing epoxy and 0.1 mm glass spacers. This allowed for the oil-water system to achieve hydrostatic equilibrium, ensuring that a planar oil-water interface could be attained via the addition or removal of water from the outer portion of the sample cell.

After forming a planar oil-water interface free of any solutes, an oil droplet containing tracer particles was directly added to the upper oil phase of the sample cell. This yielded a seeded tracer concentration of ~$4\times10^6$ particles-cm$^{-2}$ at the interface, a concentration which was necessary for accurate particle tracking measurements and quantifying the interfacial spreading velocities resulting from the introduction of surfactant. It should be noted that at this concentration, seeded tracer particles displayed slight aggregation. Very large aggregates would be expected to display lower interfacial spreading velocities in comparison to unaggregated primary particles due to their larger mass and could therefore introduce some degree of uncertainty into the measured interfacial spreading velocities in this experimental setup. However, the largest aggregates observed in this study consisted of 2-3 primary particles, and measurements of the steady-state, fully developed displacement rates for these aggregates were indistinguishable from the measured displacement rates of unaggregated, interfacially adsorbed primary particles.

Following the seeding of tracer particles, the experimental cell was stabilized for 15 minutes, then a 10 μL droplet of either surfactant solution was formed at the tip of a metal capillary

within the oil layer. The droplet was equilibrated for an additional 30 minutes within the upper oil layer prior to contact with the planar oil-water interface to allow for saturated interfacial adsorption of the surfactant. Finally, the droplet was lowered slowly (~0.01 mm $s^{-1}$) to contact the planar oil-water interface and the resulting isotropic tracer particle motion was captured using an inverted microscope and high-speed camera (Photron Mini UX) at 2000 frames per second. Due to the remarkably high energy of attachment for micrometer-scale particles at the oil-water interface, [40] particle motion was presumed to be approximately two-dimensional for the duration of particle spreading. Care was taken to quantify the displacement of at least five tracer particles from two separate experiments for each oil-water-surfactant system, measured manually using ImageJ software.

## 3. Results and Discussion

### *3.1. Effect of surfactant type on bridge expansion and bulk mixing during the coalescence of equally sized drops*

Our investigation of surfactant contributions in the generation of opposing flows within coalescing binary droplets begins with the consideration of two surfactant-free droplets sharing an equivalent initial diameter, 2R (= 2 mm), and approximately equal oil-water interfacial tensions (surfactant-free, undyed droplet: $\gamma_1$ = 23.67 ± 0.13 mN $m^{-1}$; surfactant-free, dyed droplet: $\gamma_2$ = 21.42 ± 0.27 mN $m^{-1}$). Analysis of bridge expansion for the two, equally sized coalescing droplets with no added surfactant revealed that this system closely obeyed the $D_b/2 \propto (R\gamma/\rho_{out})^{1/4} t^{1/2}$ scaling relation over the entire duration of droplet merging (Figure 4), agreeing well with the experimental observations of previous researchers. [17,18]

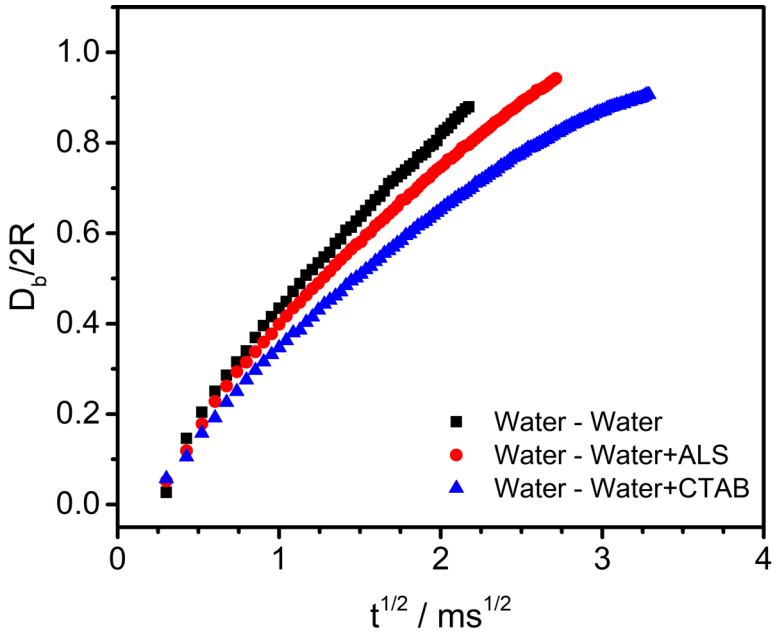


**Figure 4.** Kinetics of expansion for the connective bridge separating spherical droplets with an equivalent initial diameter, 2R (= 2 mm). The data represent the increase in the connective bridge diameter, $D_b$, relative to 2R, as a

For equally sized coalescing droplets, where one of the drops contained $2.5\times10^{-3}$ mol $L^{-1}$ ALS, the $D_b/2 \propto t^{1/2}$ scaling relation was also closely obeyed, but a slightly reduced slope in the experimental data was observed. This indicates that the value of the prefactor, $(R\gamma/\rho_{out})^{1/4}$, in the coalescence scaling relation was influenced by the presence of ALS. Likewise, an even more pronounced decrease in the slope of this scaling relationship became apparent at longer times for systems containing $2.5\times10^{-3}$ mol $L^{-1}$ CTAB. This further suggests that the gradient in interfacial tension and timescale of solutal Marangoni flow of the chosen surfactant along the interface of expanding liquid bridge has a demonstrable influence on the value of the prefactor in the scaling relation, which was not explicitly accounted for or discussed in the derivation of this scaling relation.

The characteristic time scale for coalescence of two equally sized drops with equal interfacial tensions in inviscid flow is set by $\tau_C = \sqrt{(\rho R^3)/\gamma}$. [41] For the merging of two 0.75-mm radius water drops in the inertial regime, with $\gamma = 23$ mN m$^{-1}$, $\tau_C$ is ~4.2 ms. This characteristic relaxation time closely approximates the experimentally measured time required for the expanding bridge between the surfactant-free water droplets to become equal to the initial drop diameter for the system shown in Figure 5a. This approximation is less representative in the presence of a surfactant concentration gradient, which can be seen from the data in Figure 5b and 5c, for ALS and CTAB, respectively. Each of these systems require a longer duration for the diameter of the

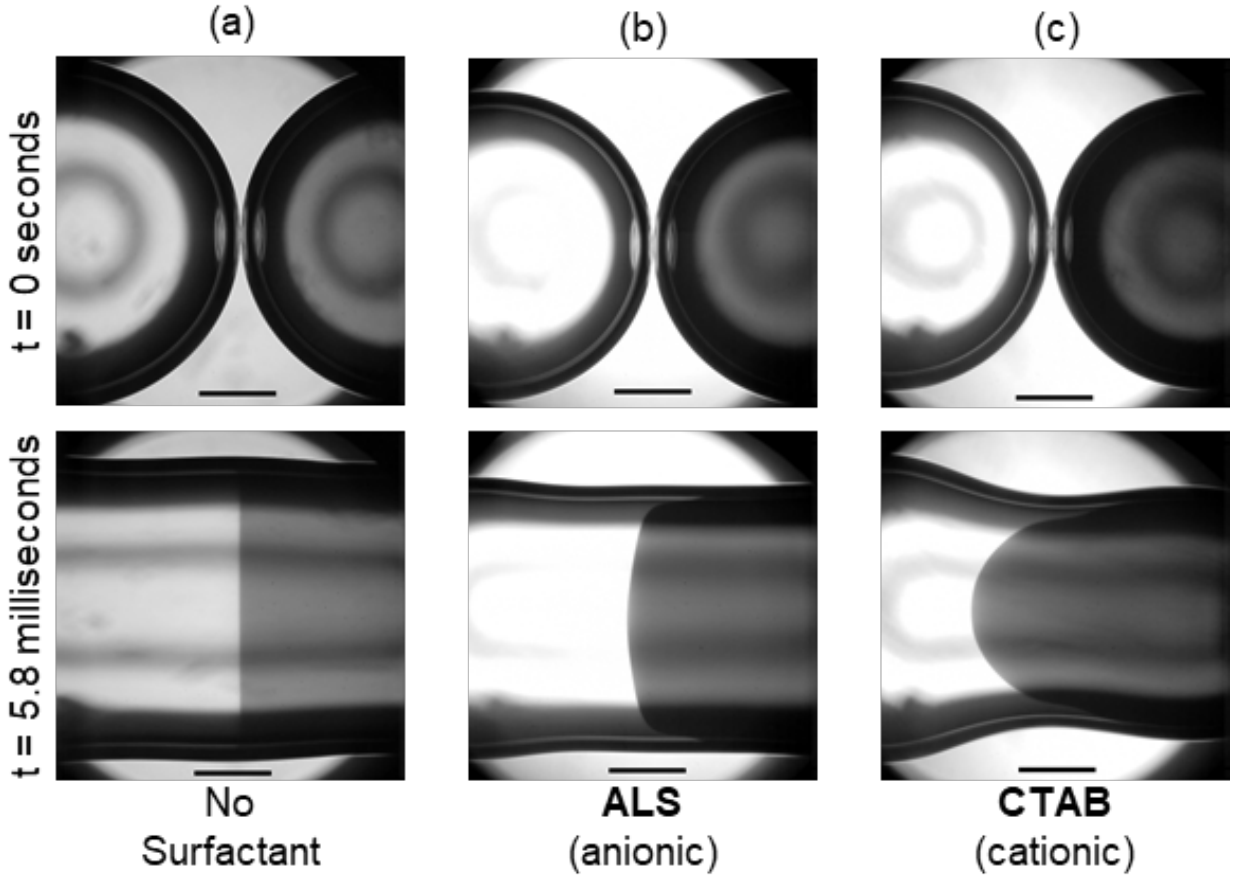


**Figure 5.** Temporal shape profiles of equally sized water droplets coalescing in triglyceride oil. The leftmost droplet in each image contained either (a) no surfactant, (b) $2.5\times10^{-3}$ mol L$^{-1}$ ALS, or (c) $2.5\times10^{-3}$ mol L$^{-1}$ CTAB, while the rightmost droplet in each image was surfactant-free, with dye added for flow visualization. The absence or presence of opposing flows at the interface and within the bulk of the merging droplets illustrate the effect of interfacially adsorbed surfactant molecules. Differences in the curvature of the jetted fluid following coalescence in (b) and (c) demonstrate the influence of surfactant headgroup architecture on the relative magnitude of these induced flows. The scale bars in each image are 0.5 mm in length.

expanding bridge to be equal to the initial diameter of the drops. The observed increase in $\tau_C$ for systems containing ALS or CTAB, as well as the clear difference between their corresponding $\tau_C$ values, suggests that interfacial adsorptive and convective properties of the surfactant contribute to the decrease in the value of the prefactor in the coalescence scaling relation. This observation is discussed in greater detail in Section 3.3.

Figure 5a illustrates that negligible internal mixing occurred during the merging of surfactant-free droplets due to the generation of two balanced, plug-flow water jets which converged at the propagating coalescence neck. In this instance, the interfacial tensions of the converging droplets are balanced and thus no tangential stress was competing with the bulk fluid motion of the merging drops. This behavior agreed well with experimental observations of previous researchers. [17,18] Contrarily, coalescence of binary droplets with non-uniform compositions of a surface-active species displayed pronounced internal convective mixing during the coalescence process, the degrees of which strongly depended on the surfactant present at the oil-water interface of the surfactant-laden droplet.

Distinct bulk fluid motion was observed in the presence of either anionic ALS or cationic surfactant CTAB for equally sized droplet with a capillary pressure ratio of $\Delta P_2/\Delta P_1 \approx 5$ (where $\Delta P_1$ and $\Delta P_2$ are the capillary pressures of the leftmost droplet and the rightmost droplet, respectively) and are shown in Figures 5b and 5c. The presence of surfactant in the undyed, leftmost drop led to the formation of a fluid jet which propagated from the bulk of dyed, surfactant-free drop as direct result of this droplet's higher capillary pressure. For the binary droplets system containing $2.5\times10^{-3}$ mol $L^{-1}$ ALS, the motion of the jetted fluid appeared to occur under near plug flow conditions, with some discernable curvature of the jetting dyed fluid at later times. However, the internal mixing for the binary systems containing $2.5\times10^{-3}$ mol $L^{-1}$ CTAB was demonstrably

292 more pronounced, displaying a much higher curvature of the jetted fluid at later stages of
293 coalescence (i.e., after 5.8 milliseconds).

294 *3.2. Influence of surfactant type on the development of bulk fluid jetting*

295 To further aid in illustrating the marked influence of surfactant in the jetting behavior
296 observed for binary droplet systems, the initial diameters of the two merging droplets were
297 modulated by increasing the initial diameter of the leftmost droplet to 2.2 mm and decreasing the
298 initial diameter of the rightmost droplet to 1.0 mm. Figure 6a shows that for asymmetrically sized
299 droplets, both free of any added surfactant and of approximately equal interfacial tension, droplet
300 merging led to only slight jetting of the fluid within the smaller diameter, surfactant-free droplet
301 into the larger droplet as a direct result of the relatively small capillary pressure gradient ($\Delta P_2/\Delta P_1$
302 $\approx 2$) originating from the difference in initial droplet sizes. However, the magnitude of the capillary
303 pressure gradient was insufficient to induce a great deal of internal mixing.

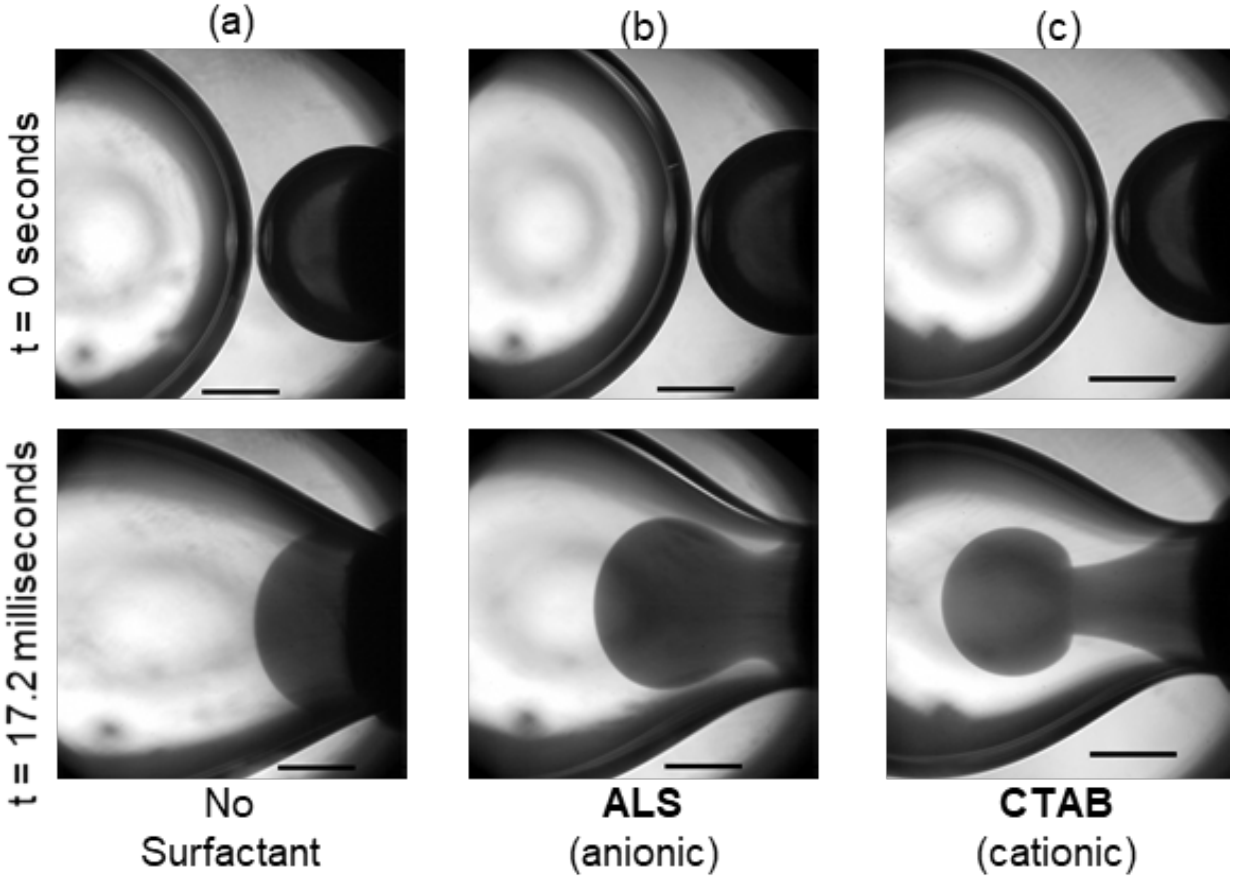


**Figure 6.** Flow profiles depicting the formation of fluid jets of different sizes for asymmetrically sized water droplets coalescing in triglyceride oil. The leftmost droplet in each image contained either (a) no surfactant, (b) $2.5\times10^{-3}$ mol $L^{-1}$ ALS, or (c) $2.5\times10^{-3}$ mol $L^{-1}$ CTAB, while the rightmost droplet in each image was surfactant-free, with dye added for flow visualization. The scale bars in each image are 0.5 mm in length.

In the case of binary droplet systems that contained a concentration gradient of either ALS or CTAB, the difference in diameter and interfacial tension between the binary droplets provided a much larger capillary pressure ratio ($\Delta P_2/\Delta P_1 \approx 11.5$) and thus a greater driving energy for jetting of the fluid from the smaller droplet into the larger droplet containing surfactant during coalescence. The late-stage flows that emerged under these experimental conditions are shown in Figure 6b and 6c, respectively. For the binary droplet system with $2.5\times10^{-3}$ mol $L^{-1}$ ALS present in the surfactant-laden droplet, the profile of the fluid jetted from the smaller, surfactant-free droplet took the shape of a bulb-like plume with a relatively large diameter forming near the apex of the jetted fluid and slightly narrower base. Similarly, for the binary droplet system containing

313 $2.5\times10^{-3}$ mol $L^{-1}$ CTAB, the late-stage internal flow also resulted in the formation of a fluid jet
314 with a large bulb and narrow base. However, the jetting that occurred in this case was demonstrably
315 stronger, with the formation of a mushroom-shaped plume of dyed water and a far narrower base.

316 The difference in the shape of the jetted fluid that emerged in systems containing ALS or
317 CTAB stemmed from the magnitudes of the convective mixing generated by the opposing bulk
318 and Marangoni interfacial flows upon droplet coalescence. As the fluid from the dyed droplet
319 flowed through the propagating coalescence neck, an interfacial diffusional flux developed in the
320 opposite direction, as interfacially adsorbed surfactant molecules in the surfactant-laden droplet
321 migrated from regions of high concentration to low concentration. This in turn generated eddy
322 currents within the bulk of the merging droplets, just beneath the interface. In the case of CTAB,
323 the driving energy for interfacial flux appeared to be sustained for a longer time than in the case
324 of ALS, which led to more pronounced eddy currents and thus the observed jetting behavior.

Furthermore, assessment of the displacement of the jetted fluid apex as a function of time for asymmetrically sized binary droplet systems, containing either ALS or CTAB (Figure 7), indicates a clear difference in the induced fluid motion. The rate of fluid jetting during the initial stages of coalescence was roughly 30% faster for the droplet system containing cationic CTAB compared to the analogous system containing anionic ALS (9.08 mm $s^{-1}$ and 6.37 mm $s^{-1}$, respectively, from a linear regression fit to the initial data in Figure 7). In the following sections, we discuss in detail our experimental basis for attributing differences in the emerged jetting phenomena to differences in the magnitudes of the induced interfacial Marangoni flows accompanying each surfactant. The jetting phenomena observed between merging drops with an

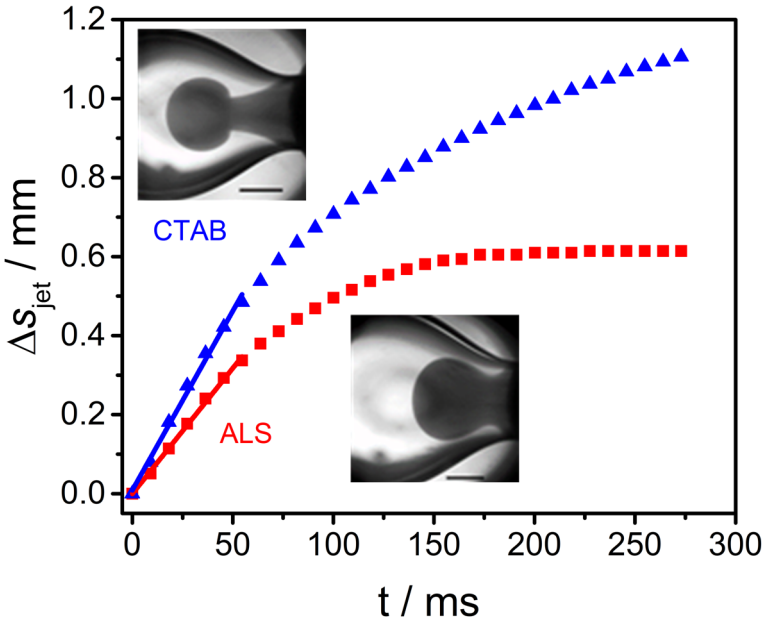


**Figure 7.** Displacement of the jetted fluid apex, $\Delta s_{jet}$, apex originating from the surfactant-free droplet into the surfactant-laden droplet as a function of time, t, succeeding droplet contact for asymmetrically sized droplet systems. Micrograph insets depict the position of the fluid jets 17.2 ms after the onset of coalescence. The scale bars in each image are 0.5 mm in length.

induced surfactant concentration gradient can also be explained by the induction of Marangoni convection, where low interfacial tension liquid along the oil-water interface of the coalescing neck is carried toward the higher interfacial tension regions in the surfactant-free droplet and

accumulates. A localized increase in the hydrostatic pressure of this region follows and the development of a bulk flow of liquid from the surfactant-free droplet in the opposite direction of the Marangoni flow.

### *3.3. Comparison of adsorptive properties of ALS and CTAB at the triglyceride oil – water interface*

Values for the surface excess concentration, $\Gamma_m$, in Table 1 indicate that CTAB molecules pack more densely at the triglyceride oil-water interface than ALS molecules, which is in line with previous experimental observations for the same or similar ionic surfactants at the oil-water interface. [42,43] The negatively charged moiety of 1:1 anionic surfactants leads these molecules to have a relatively large hydrodynamic diameter in comparison to cationic surfactants, which have a comparably small hydrodynamic diameter surrounding their positively charged headgroups. [44] These differences in the hydrodynamic volume surrounding the hydrophilic portions of each surfactant molecule lead to differences in their corresponding equilibrium adsorptive capabilities at immiscible fluid interfaces. As a direct result, anionic surfactants tend to pack less efficiently at fluid interfaces than their cationic counterparts.

Each of the experimental observations of the differences in the magnitudes of solutal Marangoni convection for ALS and CTAB would also suggest that $\Gamma_m$ has a pivotal role in the timescale of Marangoni interfacial flow. A more densely packed interfacial layer laden with surfactant would be expected to behave more rigidly in response to interfacial tension and surfactant concentration perturbations. This rigidity restricts lateral surface movements and solutal Marangoni convention. Thus, the timescale for solutal Marangoni flow would increase, as the interface overall would take longer to relax to a homogenous state (i.e., regions of high interfacial tension and regions of low interfacial tension would exist longer for more densely packed

interfaces). Under these conditions, the high interfacial tension regions would apply a high tangential surface stress over a longer duration.

Likewise, considering that both ALS and CTAB are soluble in the aqueous phase, and can therefore adsorb and desorb from the bulk aqueous phase during droplet coalescence, both the surfactant's diffusion coefficient, *D*, and bulk surfactant concentration, c, would be expected to decrease the timescale of solutal Marangoni flow. A surfactant that can diffuse swiftly to the interface from the bulk would be expected to decrease the lifetime of interfacial tension gradient, (i.e., higher diffusion coefficients will favor a small concentration difference). Similarly, high concentrations of surfactant in the bulk would be expected to increase the overall adsorption rate of molecules near the interface, thus favoring small concentration gradients and reducing the timescale of solutal Marangoni convection.

The timescale of solutal Marangoni convection, $\tau_M$, was approximated using these parameters in the equation, $\tau_M = \frac{\Gamma_m{}^2}{Dc^2}$. Incorporating the experimentally determined saturation adsorption values from Table 1, a bulk surfactant concentration of $2.5\times10^{-3}$ mol $L^{-1}$, and diffusion coefficients of $5\times10^{-10}$ $m^2$ $s^{-1}$ for ALS, [45] and $1\times10^{-10}$ $m^2$ $s^{-1}$ [46] for CTAB, the characteristic timescale of solutal Marangoni becomes ~0.2 ms for ALS and ~2 ms for CTAB. The order of magnitude difference in $\tau_M$ implies that the time required for interfacially adsorbed ALS molecules to respond and dampen interfacial tension fluctuation is far faster than that of CTAB molecules.

Regarding the flows observed in the coalescence of binary droplets with asymmetric compositions, the differences in interfacial motion between surfactants can be directly attributed to the magnitudes of the surfactant molecule's corresponding $\tau_M$ values. The timescale of solutal Marangoni convection is shorter than the characteristic coalescence timescale for two water

droplets of equal diameters and interfacial tensions in the inertial regime for ALS (i.e., $\tau_M < \tau_C$). The driving energy for solutal Marangoni-driven convection is therefore relatively low because interfacial relaxation toward a homogenous interfacial tension along the coalescing bridge occurs faster than the time required for droplets to completely merge. In contrast, these timescales are very close in magnitude for systems containing CTAB (i.e., $\tau_M \approx \tau_C$). Thus, for CTAB molecules, relaxation toward homogenous interfacial tension takes much longer and is on the order of the time required for droplets to merge, which leads to the development of strong Marangoni-driven convection and competing bulk and interfacial flows.

### *3.3. Surfactant interfacial spreading properties under an induced concentration gradient*

Figure 8 shows the distance tracer particles travel as a function of time at the (initially) pure triglyceride oil-water interface following the introduction of a $2.5\times10^{-3}$ mol $L^{-1}$ aqueous droplet solution of either anionic ALS or cationic CTAB. These data represent the fully-developed

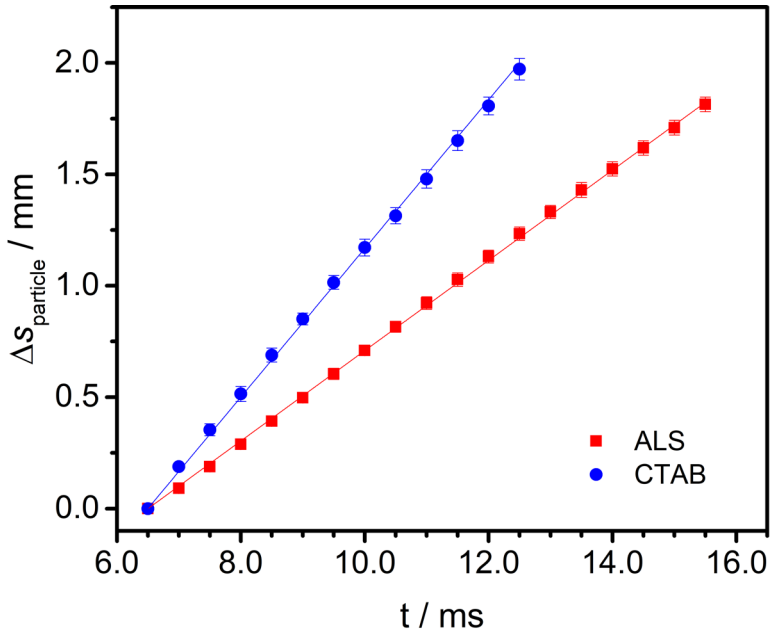


**Figure 8.** Seeded tracer particle displacement, $\Delta s_{particle}$, versus time, t, following the introduction of a $2.5\times10^{-3}$ mol $L^{-1}$ aqueous droplet solution of anionic ALS or cationic CTAB surfactant at a planar triglyceride oil-water interface. Motion of the interfacially seeded tracer particles resulted directly from the induced surfactant concentration gradient of either ALS or CTAB. Data are shown for fully developed particle displacement rates, 6.5 milliseconds after initial

393 motion of the particles, starting 6.5 ms after the introduction of surfactant into the pure oil-water
394 interface.

395 These data show a clear difference in the steady-state spreading velocities, $U_s$, of seeded
396 glass spheres under the induced concentration gradient (i.e. for ALS: $U_s = 0.202$ m $s^{-1}$; for CTAB,
397 $U_s = 0.333$ m $s^{-1}$) which implies that the surface motion driven by unbalanced interfacial tensions
398 in the presence of cationic CTAB molecules exceeds that of ALS molecules. Taking the initial
399 droplet diameter, 2R (= 2 mm), as the characteristic length scale, an estimation of the characteristic
400 timescale for the oil-water interface to deform under the induced surfactant concentration gradient
401 can be obtained from $\tau_D = 2R/U_s$. Approximations of $\tau_D$ yield 10 ms for ALS, and 6 ms for CTAB.
402 These calculations for the characteristic timescales of interfacial deformation under and induced
403 surfactant concentration gradient provide additional evidence that ALS molecules express a lower
404 driving energy for solutal Marangoni-driven convection in comparison to CTAB molecules. As
405 the driving energy for solutal Marangoni convection is lower for ALS, the overall motion of solutes
406 attached to an oil-water interface when subjected to a concentration gradient would be expected to
407 be influenced less by gradients in surfactant concentration because such gradients are short-lived.

408 The primary difference between the between measuring the interfacial spreading properties
409 that develop in a droplet-planar coalescence system as opposed to a droplet-droplet system is the
410 direction of the generated bulk flow between the aqueous droplet and planar water reservoir upon
411 coalescence. In the case of the droplet-planar interface arrangement, the capillary pressure ratio,
412 $\Delta P_2/\Delta P_1$ (where $\Delta P_1$ and $\Delta P_2$ are the capillary pressures for the surfactant-laden droplet and planar
413 water reservoir, respectively), would approach zero because of the approximately infinite radius
414 of curvature of the planar water reservoir. This would in turn produce a driving energy for bulk
415 fluid motion to propagate from the surfactant-laden droplet into the surfactant-free, planar

reservoir. This bulk fluid behavior stands in contrast to the bulk flows observed and quantified in Section 3, where bulk fluid motion was driven from the surfactant-free droplet into the surfactant-laden droplet due to the capillary pressure gradient. However, Marangoni-induced interfacial flows always act in the direction of the interfacial solute concentration gradient [19] and occur on a shorter timescale than bulk flows. Thus, the measured values for the interfacial spreading velocities (i.e. the Marangoni-induced interfacial flowrates) would presumably be minimally influenced by the experimental arrangement.

It is worth noting once again that this difference in interfacial spreading was observed for two surfactants with distinct chemical architectures, which both reduced the interfacial tension of the pure triglyceride oil-water interface to approximately 3 mN $m^{-1}$ at a high bulk concentration. The observed differences in interfacial spreading and jetting behavior during the coalescence of binary droplets with nonuniform compositional properties must be explained by additional interfacial relaxation mechanisms, which have not previously been studied in detail by the recent literature.

## 4. Summary and Conclusion

Direct observation of the bulk flows generated during the coalescence of binary water-in-oil droplets with non-uniform physical properties and characterization of the contributive surfactant-induced interfacial phenomenon was performed. Mechanisms responsible for the observed opposing interfacial and bulk flows between merging surfactant-laden and surfactant-free droplets were also described. Fluid jets that developed during binary droplet coalescence were a direct result of convection driven solutal Marangoni flows which generated a rapid redistribution of low interfacial tension bulk fluid around the perimeter of the high interfacial tension bulk fluid. The degree of interfacial spreading and bulk fluid redistribution was greater for cationic CTAB

molecules compared to ALS molecules due to stark differences in their equilibrium adsorption values, kinetic re-adsorptive rates during droplet coalescence, and overall tendency for expressing solutal Marangoni convection.

This work stands in contrast to work of previous researchers in that control over bulk flows during the coalescence of binary water droplets was induced entirely through optimized surfactant selection, with no need for modulation of the bulk viscosities of the outer or inner liquid phases. Our experimental results provide additional experimental confirmation that the governing power-law relationship for coalescing droplets in the inertial regime is obeyed in the presence of an induced surfactant concentration gradient, but the prefactor in this relationship is strongly dependent upon the interfacial properties of the added surfactant.

The analyses and relationships outlined in this work can be generalized for many different surfactant types, including anionic or cationic surfactants with longer alkyl chains than those investigated here, nonionic surfactants with various alkyl tail lengths, and zwitterionic surfactants. The parameters which are expected to shorten the timescale of solutal Marangoni-convection (while decreasing its driving energy) include the surfactant's diffusion coefficient and bulk concentration, while equilibrium interfacial saturation adsorption is the primary contributor in extending the timescale of solutal Marangoni convection. Thus, enhancing the bulk mixing of binary drops with an induced concentration gradient can be done by selecting a surfactant that packs densely at the immiscible fluid interface and adsorbs to the interface strongly. Zwitterionic and polymeric surfactant would likely be ideal candidates for such applications due to their relatively small diffusion coefficients and dense interfacial organization capabilities. [47]

One of the most advantageous applications of using the controlled coalescence of droplets with asymmetric properties is in the synthesis of functional nanoparticles. Recently, Frenz et al.

[27] demonstrated that magnetic iron oxide nanoparticles could be precipitated in a highly reproducible reaction following the fusion of droplet pairs consisting of different reagents in a hydrodynamically coupled, single-nozzle microfluidic device. Controlled pairwise mixing of aqueous droplets in oil was produced by electrocoalescence [48] and the droplets were prevented from fusing prematurely by using a uniformly distributed surfactant at the interfaces of both droplets. The methodology developed by these researchers could be readily adapted to incorporate the findings of the present manuscript by isolating the surfactant to one of the inlet droplet flows, while leaving the other surfactant-free. Upon merging, Marangoni-induced flows would produce pronounced bulk mixing between the drops, like those explored here. Moreover, enhanced control over the degree of mixing obtained between the drops at different timescales could be explored with the previously discussed surfactant selection criteria.

In this study, we proposed a simple, yet robust experimental methodology for directly quantifying the solutal Marangoni timescales of surface active compounds at the oil-water interface under an induced concentration gradient. With this method, the spreading efficiencies and encouragement of bulk fluid mixing for potentially any surfactant type at the oil water interface can be economically measured. The insights garnered from this work provide a compelling alternative route for inducing bulk flows in microfluidic devices without the need for modulating bulk phase viscosities.

**Acknowledgements**

Financial support for this work was provided by the National Science Foundation through the East Asia and Pacific Summer Institutes (EAPSI) Fellowship Program (Award Number: 1713936). The authors would also like to thank the anonymous reviewer whose thorough comments and suggestions led to a substantially improved manuscript.

## References


[1] J.D. Paulsen, Approach and coalescence of liquid drops in air, Phys. Rev. E - Stat. Nonlinear, Soft Matter Phys. 88 (2013) 1–13. doi:10.1103/PhysRevE.88.063010.

[2] J. Qian, C.K. Law, Regimes of coalescence and separation in droplet collision, J. Fluid Mech. 331 (1997) 59–80.

[3] J.D. Paulsen, R. Carmigniani, A. Kannan, J.C. Burton, S.R. Nagel, Coalescence of bubbles and drops in an outer fluid, Nat. Commun. 5 (2014) 3182. doi:10.1038/ncomms4182.

[4] J. Eggers, J.R. Lister, H.A. Stone, Coalescence of Liquid Drops, (1999) 1–37. doi:10.1017/S002211209900662X.

[5] L. Duchemin, J. Eggers, C. Josserand, Inviscid coalescence of drops, J. Fluid Mech. 487 (2003) 167–178. doi:10.1017/S0022112003004646.

[6] D.T. Wasan, The Role of Coalescence Phenomena and Interfacial Rheological Properties in Enhanced Oil Recovery: An Overview, J. Rheol. (N. Y. N. Y). 23 (1979) 181. doi:10.1122/1.549524.

[7] S. Tcholakova, N.D. Denkov, T. Banner, Role of surfactant type and concentration for the mean drop size during emulsification in turbulent flow, Langmuir. 20 (2004) 7444–7458. doi:10.1021/la049335a.

[8] A.M. Huebner, C. Abell, W.T.S. Huck, C.N. Baroud, F. Hollfelder, Monitoring a reaction at submillisecond resolution in picoliter volumes, Anal. Chem. 83 (2011) 1462–1468. doi:10.1021/ac103234a.

[9] J.H. Kim, T.Y. Jeon, T.M. Choi, T.S. Shim, S.H. Kim, S.M. Yang, Droplet microfluidics for producing functional microparticles, Langmuir. 30 (2014) 1473–1488. doi:10.1021/la403220p.

[10] A.B. Pawar, M. Caggioni, R. Ergun, R.W. Hartel, P.T. Spicer, Arrested coalescence in Pickering emulsions, Soft Matter. 7 (2011) 7710. doi:10.1039/c1sm05457k.

[11] P. Dahiya, M. Caggioni, P.T. Spicer, Arrested coalescence of viscoelastic droplets: Polydisperse doublets, Philos. Trans. R. Soc. A Math. Phys. Eng. Sci. 374 (2016) 1–13. doi:10.1098/rsta.2015.0132.

[12] K. Ward, Z.H. Fan, Mixing in microfluidic devices and enhancement methods, J. Micromechanics Microengineering. 25 (2015) 094001. doi:10.1088/0960-1317/25/9/094001.

[13] T. Tofteberg, M. Skolimowski, E. Andreassen, O. Geschke, A novel passive micromixer: Lamination in a planar channel system, Microfluid. Nanofluidics. 8 (2010) 209–215. doi:10.1007/s10404-009-0456-z.

[14] T.J. Johnson, D. Ross, L.E. Locascio, Rapid microfluidic mixing, Anal. Chem. 74 (2002) 45–51. doi:10.1021/ac010895d.

[15] T. Krebs, C.G.P.H. Schroën, R.M. Boom, Coalescence kinetics of oil-in-water emulsions

studied with microfluidics, Fuel. 106 (2013) 327–334. doi:10.1016/j.fuel.2012.10.067.

[16] A. Arbor, G. Tryggvason, The Flow Induced by the Coalescence of Two Initially Stationary Drops, Nasa Tech. Memo. (1994).

[17] E. Nowak, N.M. Kovalchuk, Z. Che, M.J.H. Simmons, Effect of surfactant concentration and viscosity of outer phase during the coalescence of a surfactant-laden drop with a surfactant-free drop, Colloids Surfaces A Physicochem. Eng. Asp. 505 (2016) 124–131. doi:10.1016/j.colsurfa.2016.02.016.

[18] E. Nowak, Z. Xie, N.M. Kovalchuk, O.K. Matar, M.J.H. Simmons, Bulk advection and interfacial flows in the binary coalescence of surfactant-laden and surfactant-free drops, Soft Matter. 13 (2017) 4616–4628. doi:10.1039/C7SM00328E.

[19] C. V. Sternling, L.E. Scriven, Interfacial turbulence: Hydrodynamic instability and the marangoni effect, AIChE J. 5 (1959) 514–523. doi:10.1002/aic.690050421.

[20] L.E. Scriven, C. V. Sternling, The Marangoni Effects, Nature. 187 (1960) 186–188. doi:10.1038/187186a0.

[21] D.T. Wasan, Destabilization of Water-in-Oil Emulsions, in: Emuls. - A Fundam. Pract. Approach, 1992: pp. 283–295.

[22] M. Saad Bhamla, C. Chai, M.A. Àlvarez-Valenzuela, J. Tajuelo, G.G. Fuller, Interfacial mechanisms for stability of surfactant-laden films, PLoS One. 12 (2017) 1–14. doi:10.1371/journal.pone.0175753.

[23] K. Szymczyk, B. Jańczuk, The adsorption at solution-air interface and volumetric properties of mixtures of cationic and nonionic surfactants, Colloids Surfaces A Physicochem. Eng. Asp. 293 (2007) 39–50. doi:10.1016/j.colsurfa.2006.07.006.

[24] B. Jańczuk, A. Zdziennicka, W. Wójcik, The properties of mixtures of two anionic surfactants in water at the water | air interface, Colloids Surfaces A Physicochem. Eng. Asp. 220 (2003) 61–68. doi:10.1016/S0927-7757(03)00060-8.

[25] S.D. Hudson, A.M. Jamieson, B.E. Burkhart, The effect of surfactant on the efficiency of shear-induced drop coalescence, J. Colloid Interface Sci. 265 (2003) 409–421. doi:10.1016/S0021-9797(03)00396-5.

[26] W.H. Weheliye, T. Dong, P. Angeli, On the effect of surfactants on drop coalescence at liquid/liquid interfaces, Chem. Eng. Sci. 161 (2017) 215–227. doi:10.1016/j.ces.2016.12.009.

[27] L. Frenz, A. El Harrak, M. Pauly, S. Bégin-Colin, A.D. Griffiths, J.C. Baret, Droplet-based microreactors for the synthesis of magnetic iron oxide nanoparticles, Angew. Chemie - Int. Ed. 47 (2008) 6817–6820. doi:10.1002/anie.200801360.

[28] H. Diamant, D. Andelman, Kinetics of Surfactant Adsorption at Fluid-Fluid Interfaces, J. Phys. Chem. 100 (1996) 13732–13742. doi:10.1021/jp960377k.

[29] K. Eliceiri, C.A. Schneider, W.S. Rasband, K.W. Eliceiri, NIH Image to ImageJ : 25 years of image analysis, Nat. Methods. 9 (2012) 671–675. doi:10.1038/nmeth.2089.

[30] D.F. Evans, H. Wennerström, The Colloidal Domain: Where Physics, Chemistry, Biology, and Technology Meet, 2nd ed., 1999.

[31] J.J. Nash, K.A. Erk, Stability and interfacial viscoelasticity of oil-water nanoemulsions stabilized by soy lecithin and Tween 20 for the encapsulation of bioactive carvacrol, Colloids Surfaces A Physicochem. Eng. Asp. 517 (2017) 1–11. doi:10.1016/j.colsurfa.2016.12.056.

[32] J.D. Berry, M.J. Neeson, R.R. Dagastine, D.Y.C. Chan, R.F. Tabor, Measurement of surface and interfacial tension using pendant drop tensiometry, J. Colloid Interface Sci. 454 (2015) 226–237. doi:10.1016/j.jcis.2015.05.012.

[33] G. Loglio, P. Pandolfini, R. Miller, A. V. Makievski, F. Ravera, M. Ferrari, L. Liggieri, Drop and bubble shape analysis as a tool for dilational rheological studies of interfacial layers, in: D. Möbius, R. Miller (Eds.), Nov. Methods to Study Interfacial Layers, Elsevier, 2001: pp. 439–483. doi:10.1016/S1383-7303(01)80038-7.

[34] K.H. Kang, H.U. Kim, K.H. Lim, Effect of temperature on critical micelle concentration and thermodynamic potentials of micellization of anionic ammonium dodecyl sulfate and cationic octadecyl trimethyl ammonium chloride, Colloids Surfaces A Physicochem. Eng. Asp. 189 (2001) 113–121. doi:10.1016/S0927-7757(01)00577-5.

[35] V. Mosquera, J.M. Del Río, D. Attwood, M. García, M.N. Jones, G. Prieto, M.J. Suarez, F. Sarmiento, A study of the aggregation behavior of hexyltrimethylammonium bromide in aqueous solution, J. Colloid Interface Sci. 206 (1998) 66–76. doi:10.1006/jcis.1998.5708.

[36] T.G. Movchan, A.I. Rusanov, I. V Soboleva, N.R. Khlebunova, E. V Plotnikova, A.K. Shchekin, Diffusion Coefficients of Ionic Surfactants, Colloid J. 77 (2015) 492–499. doi:10.1134/S1061933X15040146.

[37] M.J. Rosen, Surfactants and Interfacial Phenomena, 3rd ed., John Wiley & Sons, Inc., 2004.

[38] J. Eastoe, S. Nave, A. Downer, A. Paul, A. Rankin, J. Penfold, Adsorption of Ionic Surfactants at the Air - Solution Interface, Langmuir. 16 (2000) 4511–4518. doi:10.1021/la991564n.

[39] B.J. Park, J. Pantina, E.M. Furst, M. Oettel, S. Reynaert, Direct Measurements of the Effects of Salt and Surfactant on Interaction Forces between Colloidal Particles at Water−Oil Interfaces, Langmuir. 24 (2008) 1686–1694. doi:10.1021/la7008804.

[40] B.P. Binks, Particles as surfactants - Similarities and differences, Curr. Opin. Colloid Interface Sci. 7 (2002) 21–41. doi:10.1016/S1359-0294(02)00008-0.

[41] M. Wu, T. Cubaud, C. Ho, Scaling law in liquid drop coalescence driven by surface tension, Phys. Fluids. 16 (2004) 51–54. doi:10.1063/1.1756928.

[42] S.J. Rehfeld, Adsorption of Sodium Dodecyl Sulfate at Variuous Hydrocarbon-Water Interfaces, J. Phys. Chem. 71 (1967) 738–745. doi:10.1021/j100862a039.

[43] V.B. Fainerman, E. V. Aksenenko, N. Mucic, A. Javadi, R. Miller, Thermodynamics of

adsorption of ionic surfactants at water/alkane interfaces, Soft Matter. 10 (2014) 6873–6887. doi:10.1039/C4SM00463A.

[44] A. Prins, C. Arcuri, M. Van den Tempel, Elasticity of Thin Liquid Films, J. Colloid Interface Sci. 24 (1967) 84–90. doi:10.1016/0021-9797(67)90281-0.

[45] A. Javadi, N. Mucic, D. Vollhardt, V.B. Fainerman, R. Miller, Effects of dodecanol on the adsorption kinetics of SDS at the water–hexane interface, J. Colloid Interface Sci. 351 (2010) 537–541. doi:10.1016/j.jcis.2010.07.033.

[46] C. Stubenrauch, V.B. Fainerman, E. V Aksenenko, R. Miller, Adsorption behavior and dilational rheology of the cationic alkyl trimethylammonium bromides at the water/air interface, J. Phys. Chem. B. 109 (2005) 1505–1509. doi:10.1021/jp0465251.

[47] V. Seredyuk, E. Alami, M. Nydén, K. Holmberg, A. V. Peresypkin, F.M. Menger, Adsorption of zwitterionic gemini surfactants at the air-water and solid-water interfaces, Colloids Surfaces A Physicochem. Eng. Asp. 203 (2002) 245–258. doi:10.1016/S0927-7757(01)01106-2.

[48] K. Ahn, J. Agresti, H. Chong, M. Marquez, D.A. Weitz, Electrocoalescence of drops synchronized by size-dependent flow in microfluidic channels, Appl. Phys. Lett. 88 (2006). doi:10.1063/1.2218058.